SANDIA REPORT
SAND2005-6990
Unlimited Release
Printed December 2005

Laser Triggering of Water Switches in Terrawatt-Class Pulse Power Accelerators

Joseph R. Woodworth, Nathan D. Zameroski, David L. Johnson,
Gennady S. Sarkisov, James R. Blickem, David M. Van De Valde,
Robert L. Starbird, and Frank L. Wilkins

Prepared by
Sandia National Laboratories
Albuquerque, New Mexico 87185 and Livermore, California 94550

Sandia is a multiprogram laboratory operated by Sandia Corporation,
a Lockheed Martin Company, for the United States Department of Energy's
National Nuclear Security Administration under Contract DE-AC04-94AL85000.

Issued by Sandia National Laboratories, operated for the United States Department of Energy by Sandia Corporation.

Available to DOE and DOE contractors from
U.S. Department of Energy
Office of Scientific and Technical Information
P.O. Box 62
Oak Ridge, TN 37831

Telephone: (865) 576-8401
Facsimile: (865) 576-5728
E-Mail: reports@adonis.osti.gov
Online ordering: http://www.osti.gov/bridge

Available to the public from
U.S. Department of Commerce
National Technical Information Service
5285 Port Royal Rd.
Springfield, VA 22161

Telephone: (800) 553-6847
Facsimile: (703) 605-6900
E-Mail: orders@ntis.fedworld.gov
Online order: http://www.ntis.gov/help/ordermethods.asp?loc=7-4-0#online

SAND 2005-6990
Unlimited Release
Printed December 2005

Laser Triggering of Water Switches in Terrawatt-Class Pulse Power Accelerators

J. R. Woodworth, N. D. Zameroski
Pulsed Power Technologies Department
Sandia National Laboratories, POB 5800, Albuquerque, NM 87185-1193

D. L. Johnson,
Titan Pulse Sciences, 2700 Merced St. San Leandro, CA

G. S. Sarkisov, J. Blickem,
Ktech Corporation, 1300 Eubank Blvd, SE, Albuquerque, NM 87185

D. M. Van De Valde,
EG&G Technical Services, 2420 Comanche Rd. NE, Albuquerque, NM 87185

R. L. Starbird, F. Wilkins
Bechtel Nevada, Las Vegas, Nevada

Abstract

Focused Beams from high-power lasers have been used to command trigger gas switches in pulse power accelerators for more than two decades. This Laboratory-Directed Research and Development project was aimed at determining whether high power lasers could also command trigger water switches on high-power accelerators. In initial work, we determined that focused light from three harmonics of a small pulsed Nd:YAG laser at 1064 nm, 532 nm, and 355 nm could be used to form breakdown arcs in water, with the lowest breakdown thresholds of 110 J/cm^2 or 14 GW/cm^2 at 532 nm in the green. In laboratory-scale laser triggering experiments with a 170-kV pulse-charged water switch with a 3-mm anode-cathode gap, we demonstrated that ~90 mJ of green laser energy could trigger the gap with a 1-σ jitter of less than 2ns, a factor of 10 improvement over the jitter of the switch in its self breaking mode. In the laboratory-scale experiments we developed optical techniques utilizing polarization rotation of a probe laser beam to measure current in switch channels and electric field enhancements near streamer heads. In the final year of the project, we constructed a pulse-power facility to allow us to test laser triggering of water switches from 0.6- MV to 2.0 MV. Triggering experiments on this facility using an axicon lens for focusing the laser and a switch with a 740 kV self-break voltage produced consistent laser triggering with a $\pm$ 16-ns 1-σ jitter, a significant improvement over the $\pm$ 24-ns jitter in the self-breaking mode.

Intentionally left blank

Contents:

Figures:

Tables:

1. Introduction:

High-voltage water switches have been used as closing switches in high-power pulsed power drivers for several decades.[1 2 3 4 5 6] These switches may hold off voltages of several megavolts and then pass currents of several hundred thousand amperes during sub-microsecond power pulses. These switches are normally operated in the untriggered or self-breaking mode. The timing jitter associated with these self-breaking water switches can lower the peak voltage or current in multi-module accelerators that add voltage or current pulses from these modules either in parallel or in series. [7 8]

Some authors have reported success in command triggering oil and water switches by focusing a laser beam directly on one switch electrode.[9 10] Lischer et al.[11] and Chu et al.[12] have jointly reported laser triggering of a ~0.6-MV water switch using 4 Joules of ruby laser energy by focusing the laser beam in the water between the electrodes. Recently, Vyuga et al. have demonstrated laser triggering of a liquid switch filled with a fluorinated dimethylcyclohexane.[13]

In this Laboratory-Directed Research and Development Project, we investigated whether focused beams from relatively small Nd:YAG pulsed lasers operating at 1064 nm or a harmonic of this wavelength could be used to command trigger the water switches in large pulse-power accelerators.

This report is divided into four sections: 1. Introduction; 2. Water breakdown experiments with focused laser beams; 3. 170-kV laser-triggered water switching experiments; 4. Polarimetry experiments in which rotation of polarization in probe laser beams was used to measure electric and magnetic fields and; 5. 600-kV to 2-MV laser-triggered water switching experiments.

2. Water Breakdown Studies.

2.1 Transmission of laser light through water

In order to focus a laser beam to a breakdown arc in a water switch experiment, light of the wavelength of the laser beam must propagate an appreciable distance through pure water. Using harmonic conversion crystals, small Nd:YAG lasers can generate intense laser beams with wavelengths of 1064 nm(near infrared), 532 nm (green), 355 nm (near ultraviolet), and 266 nm (ultraviolet). Measurements we made of pure water taken directly from the Z accelerator tank suggest that the 1/e absorption length of pure water at 266 nm is about 50 cm. Measurements at the other wavelengths of interest are available in the literature[14 15]. Absorption measurements at all four wavelengths are displayed in **Table I**. To trigger a water switch, laser radiation normally has to be introduced to the inside of a high-voltage water pulse-forming line. The relatively long 1/e absorption lengths of water at 355 and 532 nm suggest that laser beams at these wavelengths could be transported directly through water from the ground side to the

high-voltage side of a pulse-forming line (PFL). The short 1/e absorption lengths at 1064 and 266 nm suggest that a gas-filled "laser-crossover tube" would be required to transport beams at these wavelengths to the inside of the pulse-forming line.

Table I: Transmission of pure water versus wavelength

Wavelength (nm)	Absorption Coefficient (cm^{-1})	1/e Absorption Length (m)	Source
266	0.02	0.5	This work
355	8.4×10^{-5}	110	Buiteveld
532	4.45×10^{-4}	22.5	Buiteveld
1064	0.12	0.08	Curico

2.2 Breakdown thresholds.

Breakdown thresholds were measured by focusing laser beams of various wavelengths into a cell filled with pure water using a 15-cm focal length lens. We defined breakdown as a visible spark in the water an audible 'pop" from the cell. To determine threshold intensities, we measured the laser pulse-lengths (typically 6 to 10 ns) with a fast photodiode. We measured the focal spot sizes of the laser beams by focusing the laser through the water cell at low laser energy and recording the energy transmitted to a calorimeter beyond the water cell as a knife-edge was slowly moved through the focal spot in 5-to-10 micron increments. Measurements were taken in two orthogonal directions and the focal spots were approximated as ellipses. **Figure 1** shows the results of a typical measurement at 532 nm. **Table II** summarizes these breakdown threshold measurements. Note that we were unable to form a breakdown arc in water with the 266 nm laser beam. In the breakdown threshold measurements at 1064 nm, the threshold given is the actual intensity at the focal spot. We have accounted for the absorption of the laser light by the water. The rise in the breakdown threshold in going from green to near UV and our inability to form a breakdown arc at 266 nm, were initially surprising. We suspect these problems with forming arcs in the UV are related to scattering of the laser light by index-of-refraction fluctuations in the water. Buiteveld et al.[14] demonstrate that this scattering becomes much worse at ultraviolet wavelengths that at visible wavelengths.

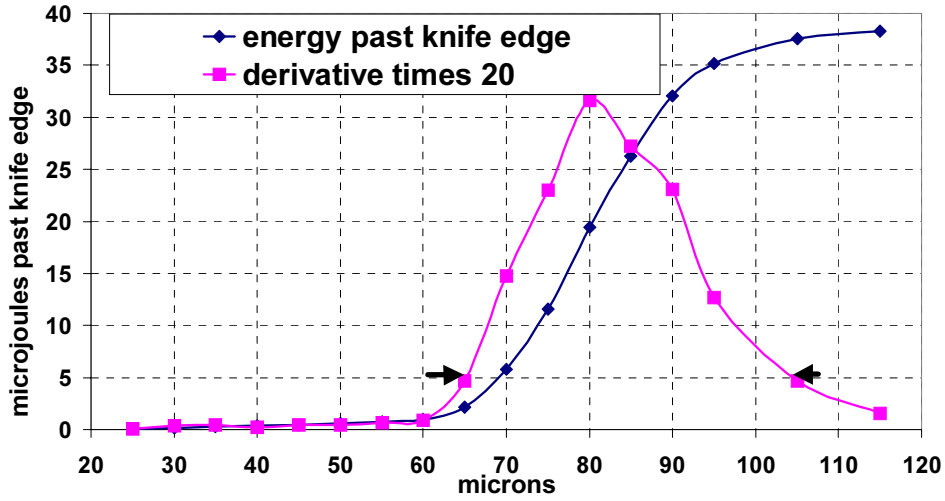

Figure 1: Results of a focal spot size measurement taken under water. The derivative curve gives the size of the focal spot. In this case, ½ of the laser energy is contained in a 40-micron spot.

Table II. Summary of laser-induced breakdown thresholds in pure water using 15-cm focal length lens. Two orthogonal measurements of spot sizes are given. Note that the laser pulse-length was 10 ns at 1064 nm but 8 ns at 532 and 355 nm.

λ (nm)	1/e spot size (μm)	Laser energy (mJ)	Breakdown threshold (J/cm^2)	Breakdown threshold (GW/cm^2)
1064	10x 15	2.7	2,200	220
532	23 x 42	1	110	14
355	25 x 40	10	1,200	150

2.3 Arc lengths in water and Coherent Raman Beams.

Figure 2 shows a picture of a breakdown arc in our water cell formed by focusing 75 mJ of green laser energy through a 29-cm focal length lens. The arc is viewed through a 10-cm diameter window and behind filters that do not transmit the laser radiation. The breakdown arc appears to be approximately 5-cm long. In addition to generating a breakdown arc, focusing the green laser beam in water generates coherent red beams aligned with the part of the laser radiation. There are seen as faint red "tails" on both ends of the breakdown arc in **figure 2**. These Raman-shifted beams at ~650 nm were generated because the intense green laser beam vibrationally excited water in its symmetric stretching mode.[16]

All of our water breakdown studies are discussed in the Paper titled "Laser-Triggered Switching" by J. R. Woodworth and D. L. Johnson on page 595 in the Digest of Technical papers of the 14th IEEE International Pulsed Power Conference held in Dallas, in June 2003.

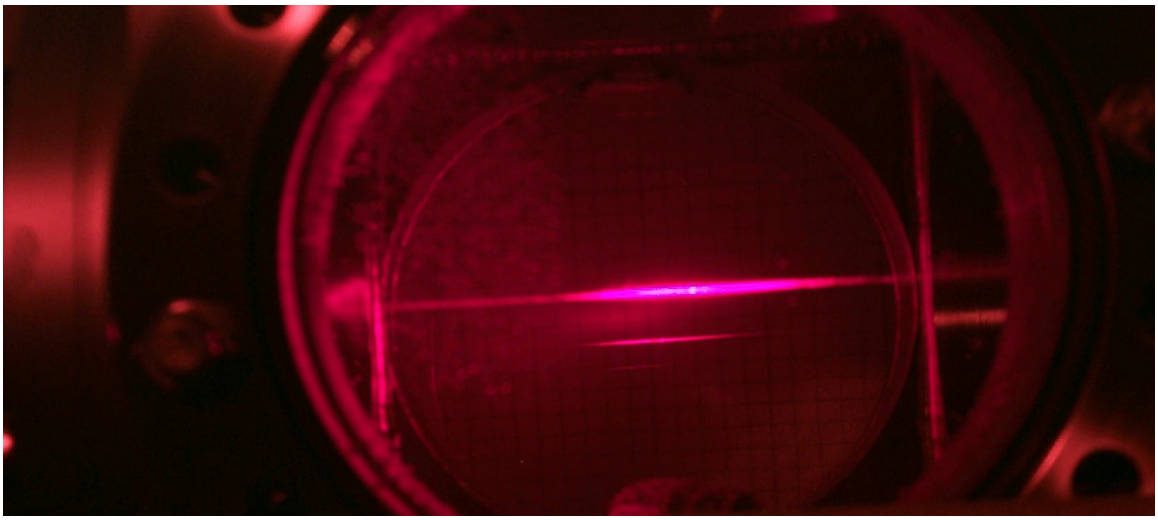

Figure 2: picture of a breakdown arc formed by focusing 75-mJ of green laser energy in water through a 29-cm focal length lens. The picture is taken through a filter that excludes the laser radiation. The arc is being viewed through a window with a 10-cm diameter.

3. 170-kV Laser-Triggered Water Switching Experiments

3.1 Apparatus

Because the results of the water breakdown experiments were encouraging, we began laser-triggered water switching experiments at 170 kV. **Figure 3** shows a schematic of our laser-triggered water switch test cell. Our cell was a hollow stainless steel cube 15-cm on a side with 10-cm diameter ports on all six sides. Two 2.5-cm diameter hemispherical electrodes separated by 3-mm formed the water switch. One electrode was connected to the high-voltage pulse generator by a high-voltage 50-Ohm cable. The opposite grounded electrode had a central 1-mm hole. The laser used to trigger the switch passed through the focusing lens and the 3.8-cm diameter fused-silica entrance window, entering the water. The laser beam passed through the 1-mm hole in the electrode, reaching focus between the electrodes and causing a breakdown arc in the water. Fused-silica windows with a 1.9-cm clear aperture were placed on opposing sides of the cell to enable optical diagnostics of the switch. A pulsed, unfocused probe laser beam at 532 nm was used to perform shadowgraphy, Schlieren photography, and polarimetry with the probe laser as the backlighting source and a CCD camera behind a 532-nm interference filter as the detector. Time resolution in these shadograms, Schlieren photographs and polarigrams was approximately 150 picosec, the pulsewidth of the probe laser. The polarimetry results, which were used to measure magnetic and electric fields in the water, are discussed in section 4.

A fiber optic cable mounted in the top of the 15-cm cube led to a fast photomultiplier tube (0.8-ns rise-time, 2 ns fall-time) in a screen room. This photomultiplier tube detected and provided timing signals from scattered light from the trigger laser and the probe laser as well as detecting visible light from the arc generated by the current pulse through the water switch.

The laser used to trigger the water switch was a flashlamp pumped, Q-switched, Nd:YAG laser with frequency multiplication crystals that allowed us to extract beams at the fundamental and several harmonic wavelengths. Output energies in the ~7 ns-wide laser pulses were ~130 mJ at the 1064-nm fundamental wavelength, ~90 mJ at the 532-nm second harmonic wavelength and ~50 mJ at the 355-nm third harmonic wavelength. The beam from the trigger laser was expanded to a 2-cm diameter before focusing to improve its focusing properties.

The high-voltage pulse generator consisted of a 2-stage mini-Marx generator in transformer oil using four 50-kV, 9-nf capacitors. Typical water switches in the large accelerators of interest to this program have voltage risetimes of 200-400 ns. We achieved a 300-ns voltage risetime on our water switch by passing the output from our mini-Marx through a 10 microHenry inductor and into a 0.5-nF peaking capacitor connected to the hot electrode of the water switch. A capacitive voltage monitor looking at the high-voltage electrode and an integrated Rogowski current monitor around the

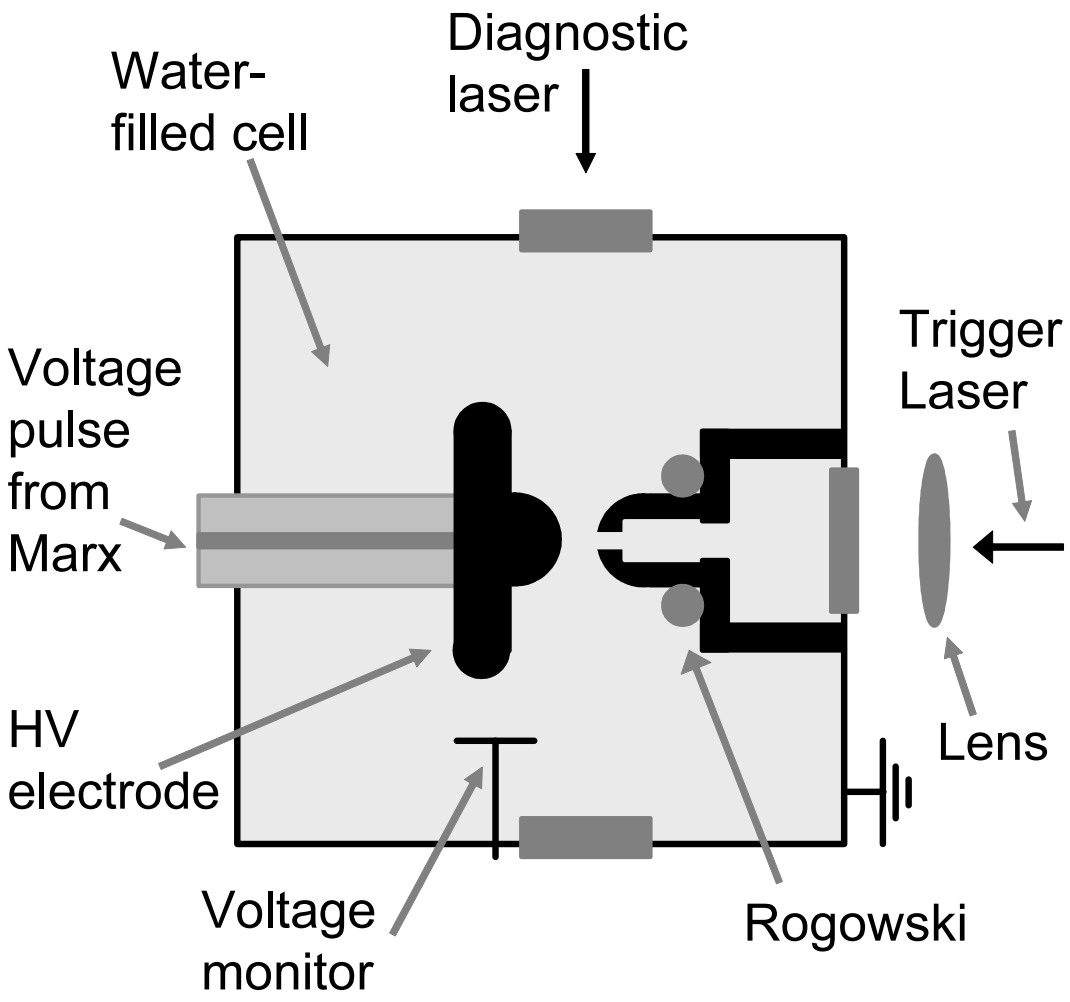

Figure 3: Apparatus for 170-kV laser triggering experiments. The laser beam entered from the right, and was focused through the hole in the grounded electrode to form a breakdown arc between the two switch electrodes.

ground electrode provided measurements of switch voltage and current. Since the ground electrode was shorted directly to our 15-cm stainless steel cube, there was no resistive damping in our peaking circuit. This resulted in a ringing current waveform after the switch closed. The high voltage pulse generator could produce either positive or negative pulses and results from experiments with both polarities are reported here.

The water was continuously deionized and degassed, with flow halted one minute before each test. Resistivity of the water was greater than 250-kilo-Ohm-cm.

3.2 Results

3.2.1 Laser Triggering Data; Current, Voltage, and Light Emission Waveforms.

Figure 4 shows a plot of switch voltage, switch current and light detected by the photomultiplier tube during one of our laser-triggered switch shots. The voltage rises for 180 ns before the infrared trigger laser beam is focused into the switch (first arrow). The switch voltage continues to rise for another 51 ns before the switch closure, shown by the voltage reduction, and current growth. Scattered light from the unfocused 532-nm diagnostic laser (second arrow) is visible on the laser-plus-light trace as the switch closes. The time between the first arrow and the start of the voltage fall is defined as the water switch delay. The slow current rise before switch closure is displacement current due to capacitive coupling across the electrode gap.

Figure 5 displays the switch delay from trigger to breakdown versus the percentage of the switch's 170-kV self-break voltage at the time of triggering. This data was generated using 85 mJ of green laser energy focused through a 7-cm focal-length lens. Most of the data falls close to a smooth curve fitted through the data, but one data point at ~73% of self-break has a significantly shorter delay. We often saw anomalously low delays when triggering the switch at voltages of ~70% of its self-break voltage or higher. While the low delay points may indicate the possibility of a low-delay, low jitter, breakdown mode at high voltages, we could not make them occur reliably. Hence we decided to avoid this mode by simply triggering at lower voltages. Excluding the point at 73% of self-break, the rest of the data has a 1-σ jitter or deviation from the smooth line through the data, of $\pm$ 1.7 ns. This is a considerable improvement over the 1- σ jitter of $\pm$ 25 ns when the switch operated in its self-break mode.

Figure 6 shows three different sets of laser-triggered water switch data we took using IR and green lasers and with 11 and 23-cm focal length lenses. All three sets of data appear to lie on the same curve of delay versus percent of self-break voltage, despite the differences in laser wavelength, lens focal length, and polarity of the high-voltage electrode.

Table III summarizes our laser- triggered water switching dataat 170 kV. Low jitter laser triggering is obtained with the long pulse (~7 ns) laser in the green and near infrared, with the lowest jitters occurring in the green with short focal length lenses (7 – 11 cm). For experiments with a 23-cm focal length lens and a negative polarity on the high-voltage electrode, higher laser energies (88 mJ vs 55 mJ) produced shorter delays and lower jitters (50 ns delay and 3.1 ns jitter at 89 mJ versus 68 ns delay and 7 ns jitter at 55 mJ). The results at different energies are consistent with visual observations that with no voltage on the switch, the focused 88-mJ beam formed a string of point plasmas almost all the way across the switch, whereas the focused 55-mJ beam formed a chain of point plasmas extending only about half-way across the switch. While the lowest jitter (1.7 ns) was obtained with a negative potential on the high-voltage electrode, no strong

dependence on polarity was seen; the switch triggered with either polarity on the HV electrode. The results with the green (532 nm) were better than the infrared triggering results even though the infrared lasers appeared to give a much more continuous laser breakdown arc than the green.

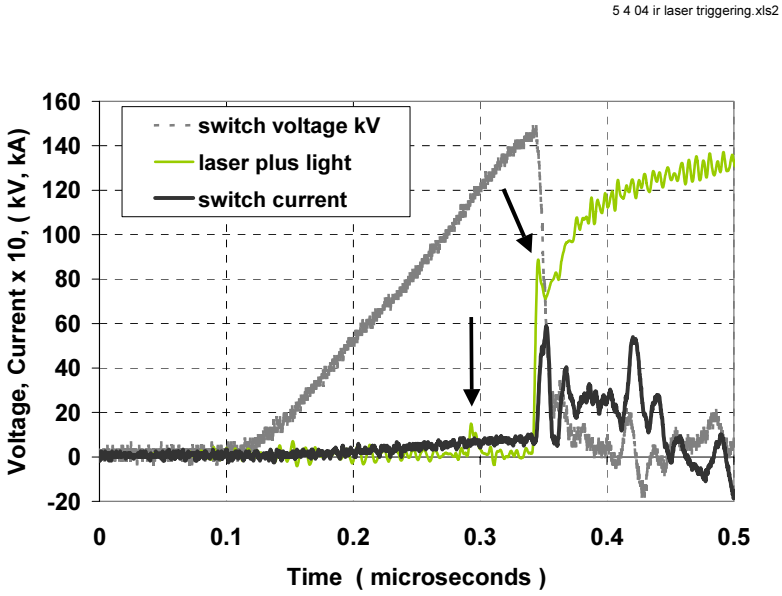

Figure 4: Plot of switch voltage, current and light emitted by the switch. The light emitted by the switch includes scattered laser radiation. Starting from the left, the first arrow indicates scattered light from the laser used to trigger the switch and the second arrow indicates light from the laser used to diagnose the triggering.

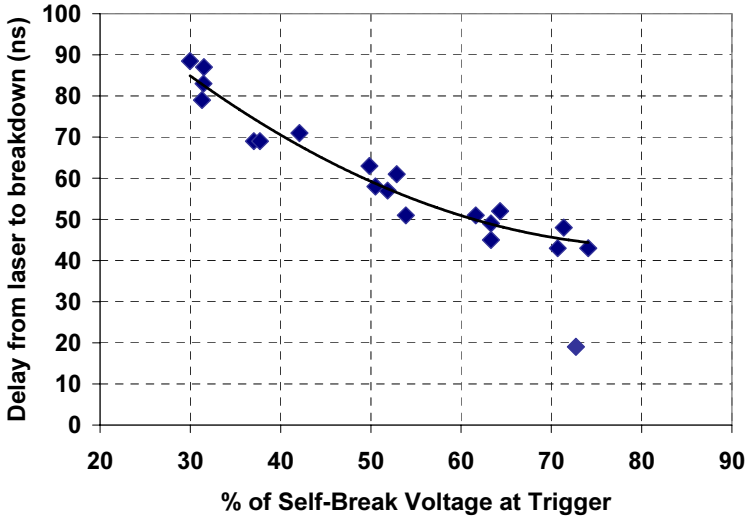

Figure 5: Plot of delay versus percent of self-break voltage at triggering time for a 3-mm gap water switch triggered with 85-mJ of green laser energy focused through a 7-cm focal length lens

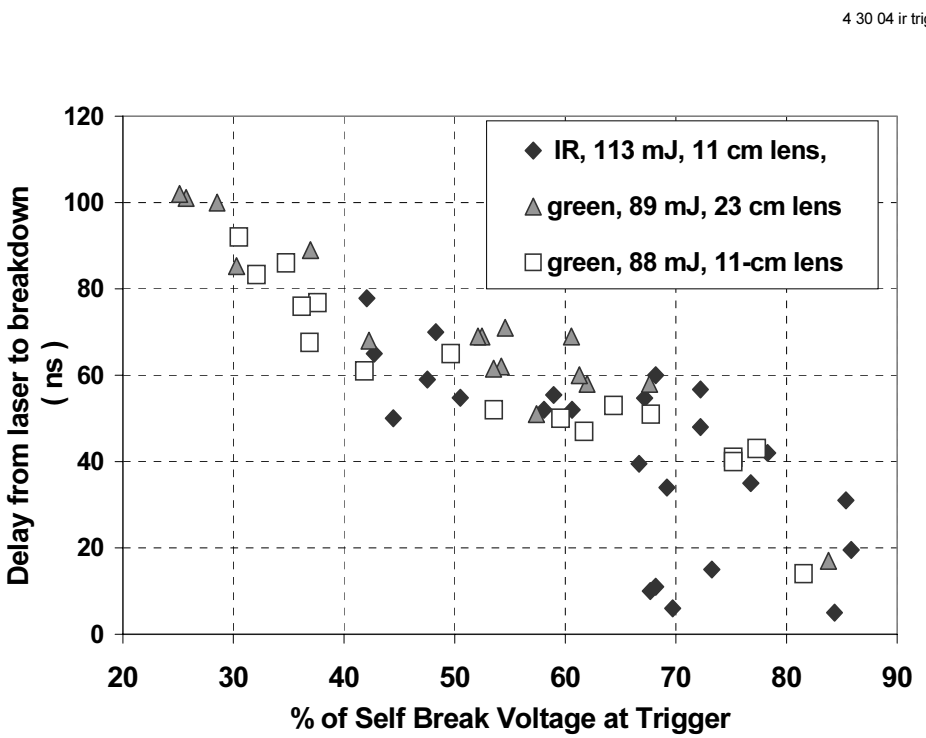

Figure 6: Plots of delay versus percent of self-break voltage at triggering time for three data sets with differing laser wavelengths and focusing lenses. Note that all of the data appears to follow the same general trend line.

Results with the short pulse (0.15 ns) laser were not encouraging. No triggering was seen with 140 mJ of 355 nm radiation. 210 mJ of green radiation produced relatively long delays and high jitters. Attempts to trigger with the 1064-nm energy from the short pulse laser generated enough stimulated Brillouin backscattering in the water to damage the laser and were abandoned. In one set of triggering experiments, 83 mJ of green laser energy from the long pulse laser was followed 50 ns later with 140 mJ of 355 nm radiation from the short pulse laser. This was an attempt to form the vapor column between the electrodes with the first laser and then ionize the column with the second laser. The results of this experiment, however, were no better than experiments using the green laser alone.

Table III: Summary of results from 170-kV laser-triggered water switch experiments.

wavelength	energy	Lens focal Length	Delay at 60% SBV	Polarity on HV electrode	1-σ jitter	Number of shots in test
(nm)	(mJ)	(cm)	(ns)	+/-	(ns)	
Long pulse; 7 ns						
532	55	23	68	-	7	5
532	85	7	50	-	4.2	8
532	85	7	50	+	1.7	20
532	89	11	50	-	2.7	16
532	89	11	57	+	3.2	20
532	89	23	55	-	3.1	18
1064	113	11	50	+	4.7	24
1064	112	23	60	+	5.0	23
Short pulse; 150 ps						
355	140	11	No triggering	-	No triggering	
532	210	11	60	-	6.5	9
Long plus 50-ns delayed short						
532 long +355 short	83 long 140 short	11	60/15	-	3.3	19

3.2.2 Laser Channel Development: Optical Diagnostic Results

No Voltage on Electrodes:

Figure 7A shows a time-integrated self-emission image of one breakdown arc with no voltage applied, using ~90 mJ of 532-nm laser energy focused through an 11-cm lens. The laser arc appears to consist of a series of "point plasmas." Figure 7B shows a laser shadowgram (532 nm, ~50 mJ, 0.15-ns backlighting laser) of the laser-induced channel and shockwaves 100 ns after the arrival of the 7-ns wide 90-mJ green trigger laser pulse. While the laser channel appears continuous in this picture, the numerous overlapping spherical shockwaves indicate that the laser channel was initially a series of discrete point plasmas, in agreement with the time-integrated picture. **Figure 7B** also shows a spherical shockwave emerging from the anode where the laser beam struck as well as a nearly planar shockwave emerging from the entire anode surface. Similar shockwaves emerging from electrodes have been seen previously in water breakdown experiments[17] and arise as a consequence of the fact that the sound speed in metal is much higher than the sound speed in water.

Bunkin et al.[18 19] suggest that the chain of point plasmas is caused by laser-induced breakdown of micro-bubbles or other "impurities" in the water. Bunkin suggests that nominally "de-gassed" water like that used in these experiments will still contain micro-bubbles. These point plasmas are unlikely to result from self-focusing of the laser beam in water since work by Feng et al. [20] indicates that a 7-ns laser pulselength is a factor of 1,000 longer than the pulselengths at which self-focusing becomes an important parameter in laser-induced water breakdown.

Figure 8 shows a sequence of four laser shadowgrams of the expanding laser channel at different times relative to the arrival of the laser pulse. Again, there was no voltage between the electrodes for this sequence. Note that the pictures were taken on four different trigger laser shots since we could only take one diagnostic shot for each pulse of the trigger laser. Figure 8 shows the transformation of the laser channel from a "needle" at 5 ns to an expanding gas channel surrounded by shock waves. The "needle" consists from linear set of hot points (see Fig.7) as indicated by the multiple overlapping spherical shock waves seen in Fig. 8B-D.

The gas column produced by the absorption of the laser energy continues to grow and coalesce until it becomes an approximately spherical bubble ~1-mm in radius 100μs after the arrival of the laser pulse. This maximum bubble diameter allows an estimate of the energy required to displace the water using the hydrodynamic relation from Cole: [21]

$$E = (4\pi/3)P_o A^3 \qquad (1)$$

Where E = energy required to displace the water and form the bubble, P_o= equilibrium pressure in the liquid and A = maximum radius of the bubble. For these experiments, the bubble is only submerged by ~15-cm of water, so the pressure is the ambient pressure of 620 Torr or 0.82 x 10^5 Pascals. This yields an energy required to form the bubble of ~0.4 mJ. Cole[22] also suggests that the shock wave will carry away about as much energy as the energy spent in forming the bubble so that the energy accounted for in the shock wave and the water displacement are on the order of 1 mJ. This is *much* smaller than the 80 – 100 mJ of incident laser energy used to produce the breakdown arcs. Visually, the light emitted by the point plasmas (at wavelengths excluding the laser wavelength) appears to be several orders of magnitude dimmer than the laser light. While our hydrodynamic analysis ignores any heating of the water caused by absorption of the laser light, it still seems likely that relatively little of the laser light is absorbed by the point plasmas, with most of the energy being either scattered or transmitted through the focal region. Any techniques that allow the focused laser energy to be absorbed more efficiently in the water would clearly be beneficial to the process of laser triggering.

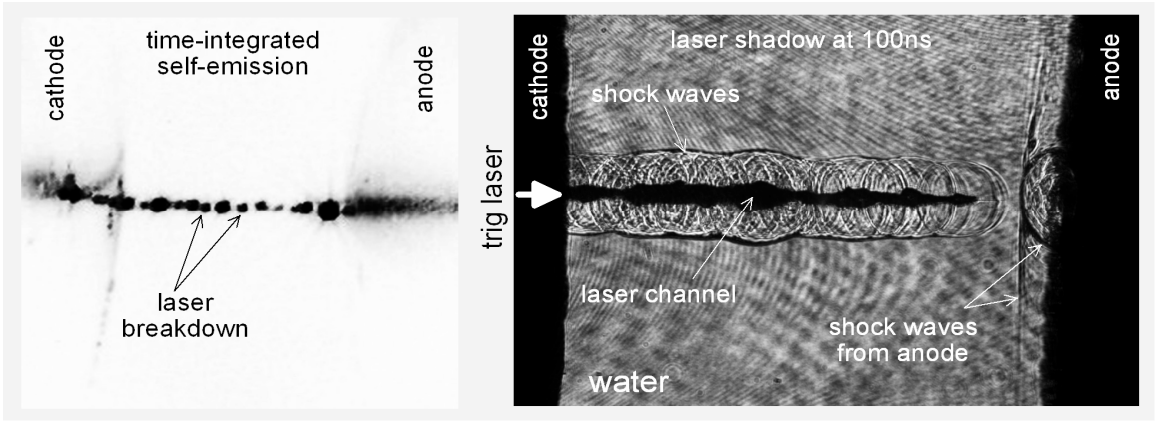

Figure 7: Right picture; time-integrated photograph of 'point-plasmas' generated between water switch electrodes by trigger laser. Left Picture; Time-resolved shadowgram of growing laser channel and shock waves taken about 50 ns after the trigger laser entered the switch. No voltage was on the switch for these pictures.

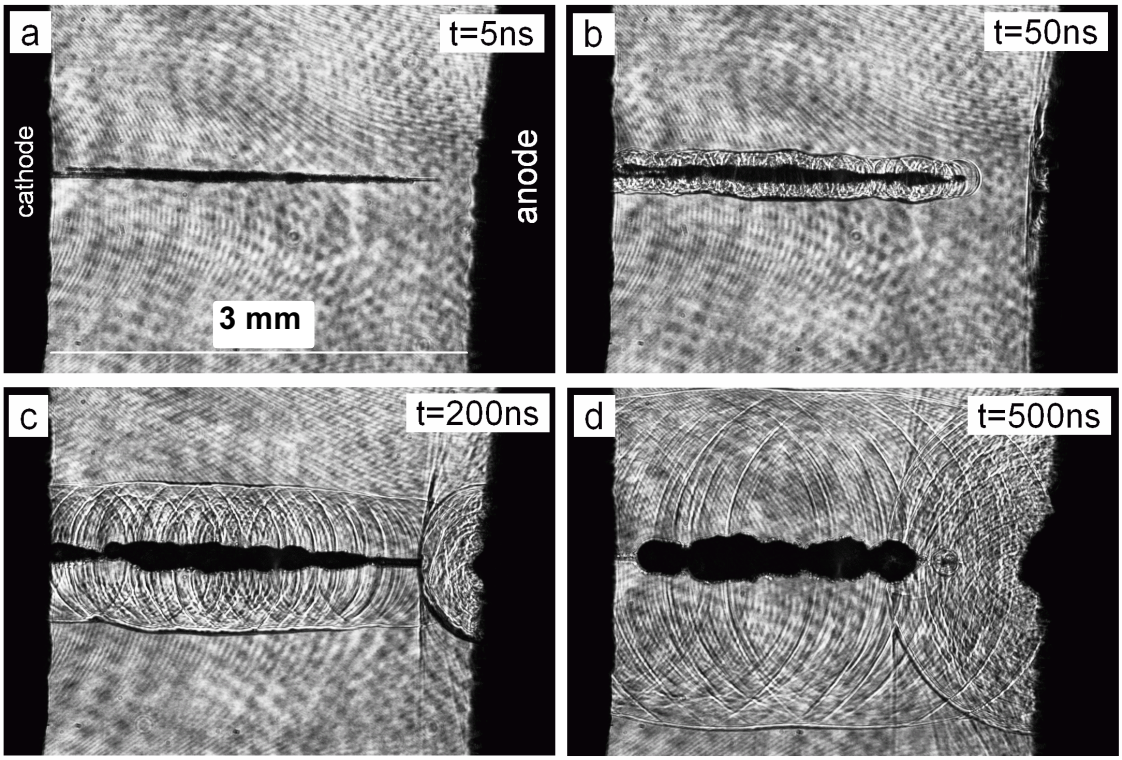

Figure 8: Shadowgrams of laser channels and shock waves at four different times.

Results with High Voltage on Electrodes:

Figure 9 shows a sequence of pictures of our laser channels taken on three different shots close to the time of switch breakdown. Early in time (Fig. 10A, 20 ns before maximum switch voltage) shows generation of the laser channel and shock waves in water. The point plasma nature of the early-time laser channel is clearly evident in this picture. In Fig. 10B, taken a few ns before switch breakdown, a number of breakdown arcs are clearly visible in the water and between different parts of the laser channel. During the voltage collapse, (Fig.9-C), the generation of a current channel in the cathode-anode gap is seen.

Figure 10 shows a time-resolved Schlieren photograph of the laser-triggered switch on another shot a few nanoseconds before breakdown. This figure demonstrates the very different nature of the laser trigger channel and the self-breakdown region in the water gap. On this shot, the laser formed a dense chain of bubbles stretching about two-thirds of the way across the gap. The laser-triggered region has completely broken down in this figure, a large streamer is reaching out from the end of the laser channel to the high-voltage electrode, and a small streamer is reaching out from the electrode to meet it. A small exploding bubble is also visible on the high-voltage electrode where some of the laser beam struck after passing through the focal region.

Figure 11 shows a streak camera image of light generated across the length of the laser-triggered switch versus time. In this case, the laser breakdown channel extended about half way across the switch. At time zero, bright scattered light from the triggering laser is seen. Next, a relatively dim plasma emission is seen from the "point plasmas". This plasma emission extinguishes in less than 10 ns as the bubbles expand into the water and cool. The switch is dark for about 10 ns as the now-cool bubbles continue expanding and merging. Much of the switch suddenly becomes luminous as the entire vapor column then breaks down in a few ns. The rest of the switch then self-breaks in another 15 ns. In addition to the streamer growing from the end of the laser breakdown column, another streamer can be seen growing from the HV electrode, possibly initiated by the fraction of the laser beam that struck the electrode. The streamer growing from the HV electrode is significantly delayed from the streamer caused by the laser channel. We speculate that this delay was caused by the fact that the laser had drilled a ~1-mm-deep hole in the electrode on previous shots and hence, this streamer started out not on the electrode surface, but in the bottom of a hole in the electrode.

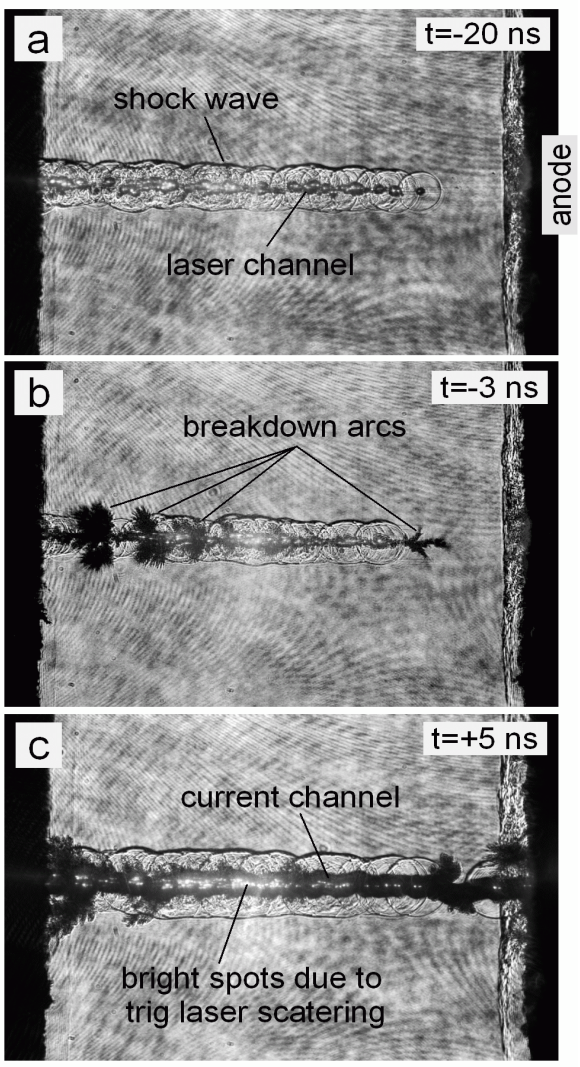

Figure 9: Shadowgrams of laser channels in the switch at three different times with voltage on the switch. Time zero is set at the start of the current pulse through the switch. Several breakdown arcs between various parts of the laser channel can be clearly seen a few ns before the start of the current pulse.

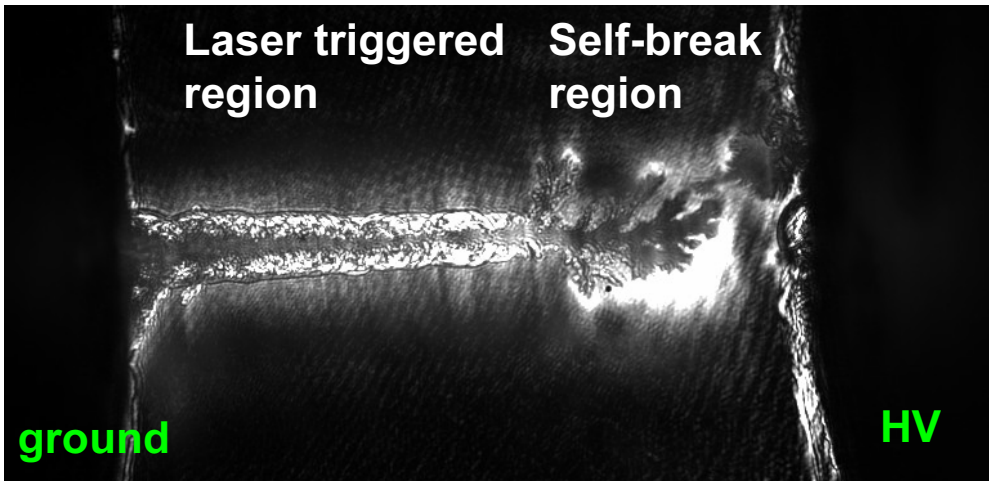

Figure 10: Time-resolved Schlieren photograph of a breakdown arc in the switch a few ns before the start of the current pulse. The laser initiated breakdown channel and the bushy self-breakdown streamer look very different.

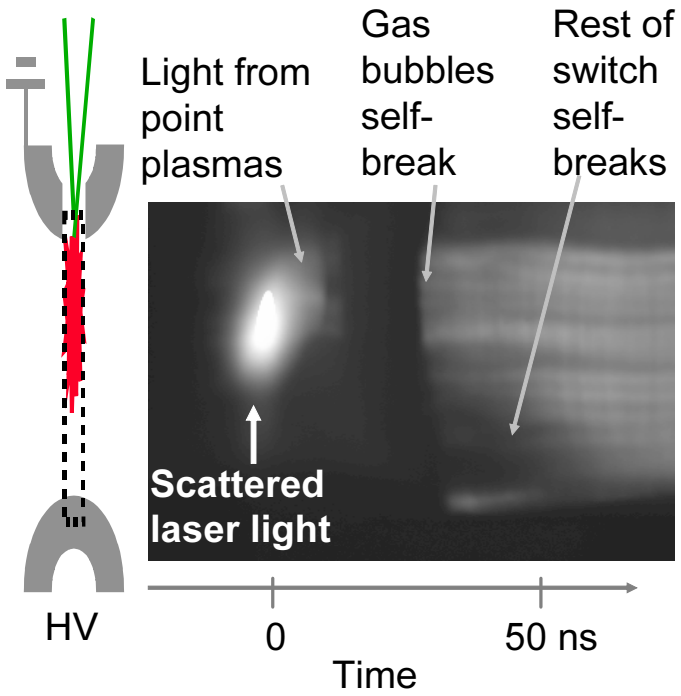

Figure 11: Streak photograph showing the time-evolution of a 170-kV laser triggered water switch breakdown.

The late-time behavior of the current carrying channel with voltage on the switch is quite different from the behavior of the laser arc alone. **Figure 12** shows four time-resolved shadowgrams of the current carrying channel in the switch and the cylindrical shock wave moving out from the core. Since the probe laser is strongly scattered by the rough water/gas interface at the outer radius of the core, the core itself appears dark. **Figure 13** plots the radii of the current-carrying core and the shockwaves versus time. Fedorov[22] and Zahn[23] suggest that the shockwaves are generated by energy deposited in the current carrying core, which becomes highly ionized during the main ~ 50 ns current pulse. The shockwaves separate from the core during the first hundred nanoseconds after the switch breaks down and continue to move outwards at 2.3 km/sec, about 1.5 times the sound speed in water. The core expands at ~.96 km/sec initially and slows to ~.24 km/sec by 900 ns.

Zahn[23] suggests that the expansion velocity of the cylindrical "core" or vapor column can be used to calculate the energy deposited in a liquid switch by the current pulse. The energy deposited in the switch is obtained by integrating the current and voltage waveforms over time. Although the short duration (~5-ns-wide) power pulse makes this calculation difficult, we conclude that about 4 Joules of energy were deposited in the water switch. In many large water-switching experiments however, the current and voltage *at the water switch* may not be known. Therefore it is useful to compare energy deposition calculations based integration of V and I curves to calculations based on the radius of the expanding cylindrical vapor column. In Zahn's paper the equation for the radius of the vapor column versus time is given as:

$$R = \alpha\, t^{0.5} \qquad (2)$$

Where R is the radius of the cylindrical vapor column, t is time, and α is given by the expression:

$$\alpha = [\, 2E/(\pi \rho_1 T(\gamma))]^{1/4} \qquad (3)$$

Here, E = energy deposited in the cylindrical vapor column per unit length, ρ_1 = the undisturbed density of liquid water and $T(\gamma)$ is an energy integral evaluated by Zahn that depends on the thermodynamic constant γ. For water vapor[24] γ = 1.31 and the resulting $T(\gamma) = 0.81$. Note from these two equations that the radius depends only on $E^{1/4}$.

From our fit to the radius of the gas column versus time, α = 0.70 $m/s^{0.5}$ Combining this with the two equations above yields a deposited energy of ~310 J/m or just under 1 J for our 3-mm arc length. Given the relatively weak dependence of radius on energy deposited and the fact that Zahn's analysis ignores the energy carried off by the shock wave, this is reasonable agreement with the 4 Joules of energy deposited as calculated from the V and I curves. In order to obtain higher accuracy measurements of energy deposited in the absence of V and I measurements, vapor column radii are needed for longer times to improve the accuracy of the fit. Peak pressures of the shock waves at known distances from the water switches would also be helpful to calculate the energy in the shock waves. Such peak pressure measurements have recently been successfully performed for multi-megavolt water switches[6].

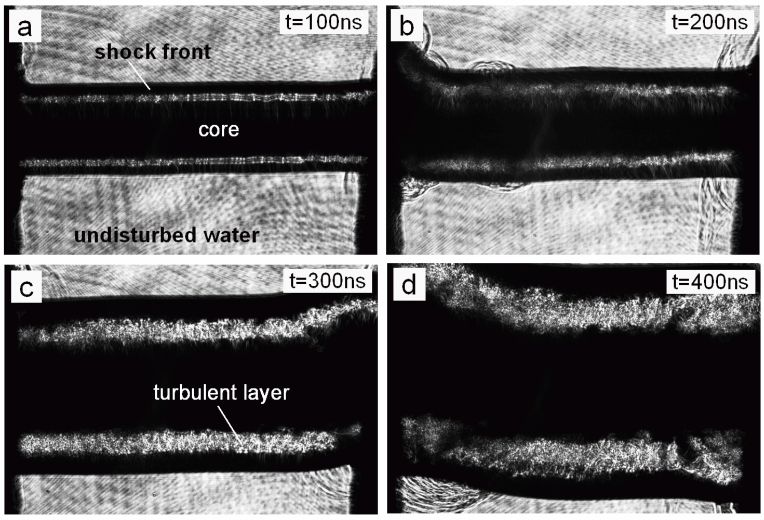

Figure 12: Shadowgrams of breakdown arcs in a 170-kV laser-triggered water switch at four different times in the current pulse.

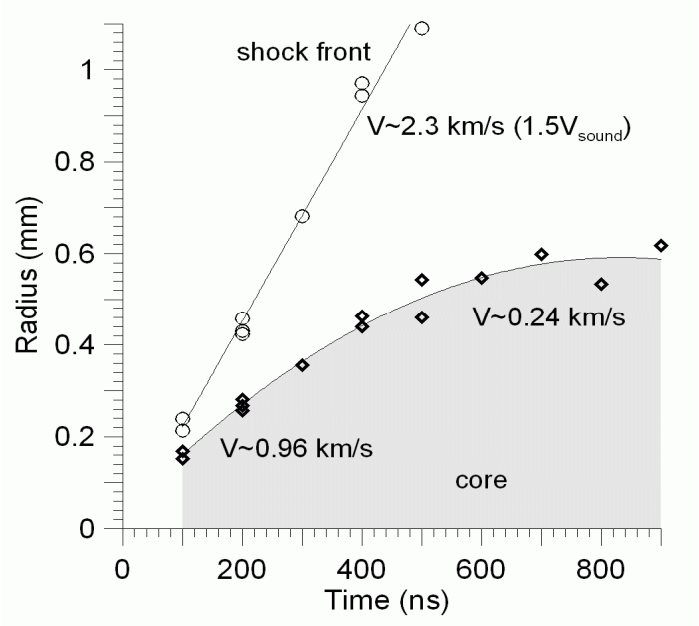

Figure 13: Radii of the current-carrying core and shock waves during main current pulse in a 170-kV laser-triggered switch.

3.3 Summary of 170 kV Triggering Results

The laser forms a string of hot dense point plasmas, probably by breaking down micro-bubbles or other impurities in the water. These point plasmas expand into the bulk water and cool quickly. They merge into a nearly continuous gas column bridging some or all of the distance between the electrodes. Effectively, a portion of the water switch is replaced with a gas switch. This gas switch, however, is highly over-volted for two reasons. First, the vapor in the "gas switch" has a density orders of magnitude lower than water and consequently has a much lower breakdown strength. Second, the vapor will have a relative dielectric constant of approximately 1, much lower than the water's dielectric constant of 81. This large difference in dielectric constants will enhance the electric fields in the vapor relative to the water. This over-volted "gas switch" breaks down rapidly, with relatively low jitter. In cases when the laser channel does not extend the entire distance between the electrodes, the remaining water-filled region acts as a self-breaking water switch after the laser channel region breaks down. The shorter the self-breaking water switch region, the shorter the delay and the lower the switch's overall jitter will be.

4. Use of the Faraday and Kerr Effects to measure current and electric field in a water-switch discharge.

In pulse-power experiments with water switches, it is important to measure current and electric field at the water switch to gain a physical understanding of the switching process. It is often difficult or impossible however, to locate standard current and voltage monitors close to the switch. In these experiments that were carried out using the 170-kV laser-triggered water switch system, we used the changing of the polarization of probing laser light passing through the switch to measure current or electric field. These measurements are described in detail in two papers[25,26] submitted to the Journal of Applied Physics and will only be summarized here.

For kilo-Ampere currents and mega-Volt/cm electric fields (which are typical for our 175 kV pulser experiments) the Kerr effect is much stronger than the Faraday effect. This would make it difficult to measure currents with the Faraday effect unless the voltage across a water switch has already collapsed to near zero as is the case in the measurements presented in section 4.1. It is possible, however, to find propagation directions and initial angles for linear polarized probe laser beam for which the Kerr effect is zero, even in the presence of strong electric fields[Error! Bookmark not defined.6]. Using this Kerr-free probing geometry one can, in principle, measure currents with the Faraday effect while there is still voltage on the water switch.

4.1 Measurement of the Current in a water switch using the Faraday Effect.

A linearly-polarized light wave propagating through water in the presence of a longitudinal magnetic field will under go a rotation in the plane of its polarization[27] by an angle α:

$$\alpha = V \int B_{II} dl \qquad (4)$$

where α is the rotation angle in deg, V is the Verdet constant in deg/G/cm, $B_{||}$ is the projection of the magnetic field on a probing direction in Gauss, and l is the probing path length. The Verdet constant for distilled water at a wavelength of 532 nm is $2.8 \cdot 10^{-4}$ deg/G/cm[28]. This B-field dependent rotation of polarization plane of probing laser beam is known as the Faraday effect. We have used this polarization rotation to measure the magnetic field around a pulsed discharge in water and hence, the current through the discharge.

The experimental setup for our measurements of both Faraday and Kerr effect are shown in **figure 14**. This shows another view of the 170-kV water switch shown in figure 4, but with emphasis on our two-channel imaging polarimeter. A short-pulse laser (Ekspla SL-312P, 532 nm, E~200-mJ, t~0.2-ns pulse width) is used to probe the water breakdown channel, functioning as a time-resolved backlighting source for the imaging polarimeter. The imaging polarimeter contains an input Glan-prism polarizer, a 3-degree calcite wedge analyzer, an imaging lens, a sheet polarizer used to compensate for differences in intensity between light in the two channels of the polarimeter, and a CCD camera. The input Glan-prism polarizer is in a high-precision rotating mount, allowing us

to precisely adjust the direction of linear polarization of the incoming probe laser beam. A lens located after the water cell focuses a backlit image of the water breakdown channel on to the CCD camera. A 3^0 calcite wedge analyzer is placed in front of the lens for angle separation of the input beam into two orthogonally-polarized beams. The lens thus forms two side-by-side images on the CCD camera corresponding to light in the two orthogonally-polarized beams.

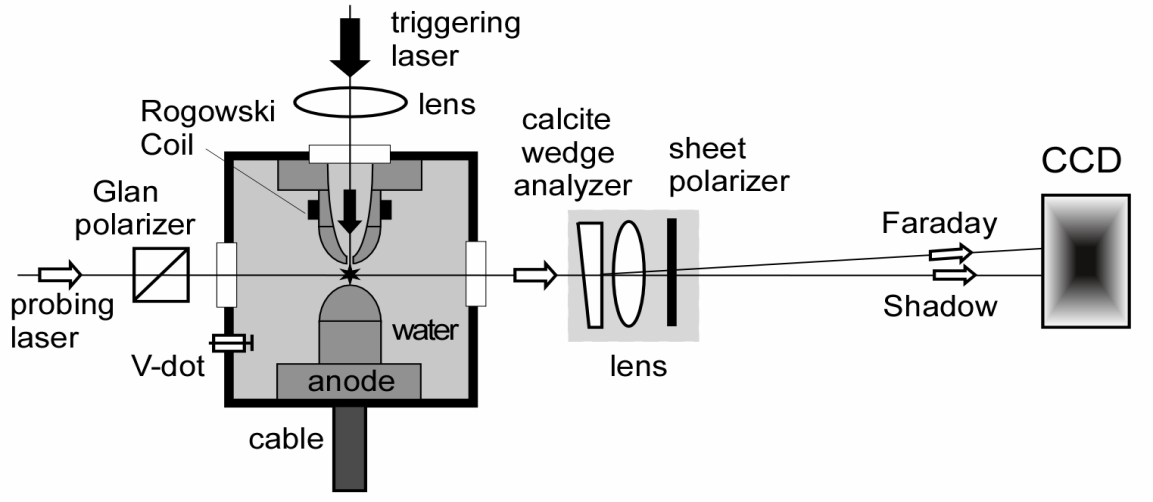

Figure 14: Apparatus for measuring magnetic and electric fields in water using Faraday and Kerr effects. The probe laser beam, which has its polarization set by the Glan prism, has its polarization modified by the electric and magnetic fields in the water. This modified polarization is detected in two pictures with orthogonal polarization on the CCD.

The Glan prism will typically be aligned so that almost all the light is in one image, called the shadowgram image. The other orthogonal channel is defined as the Faraday channel. The angle between the Glan polarizer setting and the polarization accepted by the shadowgram image is typically ~2.5 degrees for our experiments, and is defined as the "decrossing angle " and denoted by α_o. Small rotations of the polarization of the probe laser beam will shift light intensity back and forth between channels. Because almost all the light is in the shadow image, small shifts will not affect its intensity appreciably. Because the Faraday image has very little light in it (only a 2.5 degree polarization rotation would be required to shift its intensity to zero) it is very sensitive to any rotation of the polarization of the probe laser beam.

In Sarkisov et al.[25] it is demonstrated that for small polarization rotations, ($\alpha < 10°$), the rotation angle $\alpha(x,y)$ can be reconstructed as:

$$\alpha(x,y) = arcSin\sqrt{\frac{J_{0y}}{J_{0x}}(Sin^2\alpha_0 + K)\frac{J_x(x,y)}{J_y(x,y)} - K} - \alpha_0 \qquad (5)$$

where: J_{0x} and J_{0y} are the initial values of light intensity distribution in complimentary points on the Faraday and shadow images in the absence of any magnetic field and J_x and J_y are the intensity values in the presence of the magnetic field.

Figure 15 shows the results of a Faraday effect measurement during a laser-triggered shot on our 170 kV system. Since the B-fields will be in opposite directions above and below the discharge in the wire, we expect a brightening of the Faraday image relative to the shadow mage on one side of the current and a dimming of the image on the other side of the current. This is what we see in **Figure 15a**, which shows the Faraday and shadow images. **Figure 15b** shows that the probe laser recorded the picture about 80 ns after the breakdown of the voltage between the switch electrodes, at a time when the current measured by the Rogowski coil was 4.1 kA. **Figure 15c** shows the polarization rotation calculated along a path starting at point "A" as shown in 14a and stretching down past the current channel. The polarization rotation calculated is 0.65 degrees, indicating a peak current of 3.8 kA, in reasonable agreement with the value of 4.1 kA given by the Rogowski monitor. In principle, this polarization rotation technique can be used to provide a 2-dimensional map of magnetic fields (and hence currents) at one time as shown here or, with a CW laser, the technique can be used to make a continuous measurement of magnetic field along a single path length, which would provide a measurement of discharge current versus time.

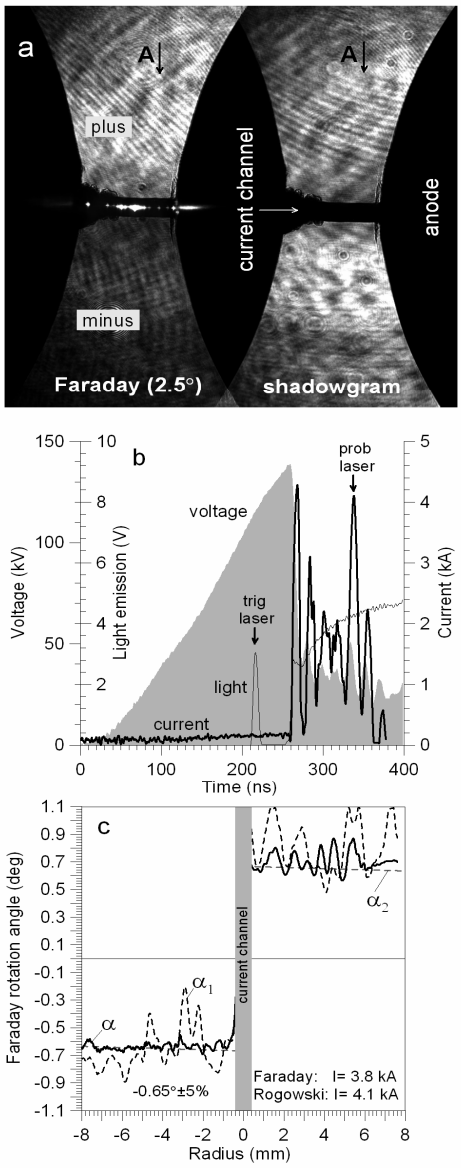

Figure 15: Results from a Faraday measurement during the current pulse after a laser-triggered gap has broken down showing; a: The Faraday and shadowgram images produced at the detector, b: a timing plot showing when the picture was taken during the current pulse and c: The polarization rotation and hence current through the channel when the picture was taken.

4.2 Measurements of the Electric Field Enhancements in a Water Switch Streamer using the Kerr Effect

The Kerr effect polarization changes caused by electric fields are both stronger and more complex than the effects due to magnetic fields. Water is normally isotropic medium, but becomes linearly anisotropic under the influence of an external electric field. The electromagnetic waves we used as a probe beam propagate through water as two normal waves with orthogonal linear polarizations. One normal wave has polarization direction along the vector *E* (ordinary wave) and the other one is perpendicular to the *E* (extraordinary wave). These normal waves propagate inside of the anisotropic medium with different phase velocities which results in a change in the polarization of the output wave. This phase shift between ordinary and extraordinary waves can be written as:

$$\varphi_K = \frac{2\pi}{\lambda}\int^{L}(n_{\text{II}} - n_{\perp})dl = 2\pi B_K \int^{L} E_{\perp}^2 dl \tag{6}$$

where φ_K is phase shift in radians, λ is the wavelength in cm, n_{II} and $n_{\perp}$ are refraction coefficients for parallel and perpendicular directions to the electric field vector, B is the Kerr constant in cm/V^2, $E_{\perp}$ is the component of external electric field which is perpendicular to the probing direction in V/cm, and L is probing path length in cm. The Kerr constant[29] for 10 MΩ-cm deionized water is $B_K = 3.4\cdot10^{-12}$ cm/V^2.

Figure 16 presents a diagram showing the orientation of the of Glan prism polarizer and the two calcite wedge analyzing axes as well as the external electric field ***E***. The probing beam wave vector ***k*** coincides with *Z* axis. The first analyzer axis coincides with *OY* direction, the second one coincides with *OX* direction. The external electric field vector ***E*** is in the *XOY* plan and contains angle $\alpha_{\boldsymbol{E}}$ with *OX* plane. The polarizer *P* axis stays in *XOY* plane at an angle α_P with *X* axis. From this geometry we can rewrite formula [1] for light intensity after the analyzer in the form:

$$\frac{I}{I_0} = Cos^2(\alpha_P - \alpha_A) + k + Sin2(\alpha_P - \alpha_E)\cdot Sin2(\alpha_A - \alpha_E)\cdot Sin^2(\varphi_K/2) \tag{7}$$

where I_0 *and* I are the light intensity before and after analyzer respectively; α_A is the analyzer angle (α_{AX}= 0 or α_{AY}= 90°), k is the sheet polarizer contrast ($k = I_{min}/I_{max} \sim 10^{-4}$). The positive sign indicates angles corresponding to counter-clockwise direction.

For our two-channel polarimeter the light intensity in *X* and *Y* orthogonal analyzer channels (α_{AX}= 0, α_{AY}= 90°) can be written as follows:

$$\frac{I_X}{I_0} = k + Cos^2(\alpha_P) + Sin2(\alpha_P - \alpha_E)\cdot Sin2(\alpha_E)\cdot Sin^2\left(\frac{\varphi_K}{2}\right) \tag{8}$$

$$\frac{I_Y}{I_0} = k + Sin^2(\alpha_P) - Sin2(\alpha_P - \alpha_E) \cdot Sin2(\alpha_E) \cdot Sin^2\left(\frac{\varphi_K}{2}\right) \tag{9}$$

Note that if the polarization of the probe beam is along the electric field vector ($\alpha_p = \alpha_E$) then the intensity ratio is not affected by φ_k and hence is not affected by the electric field.

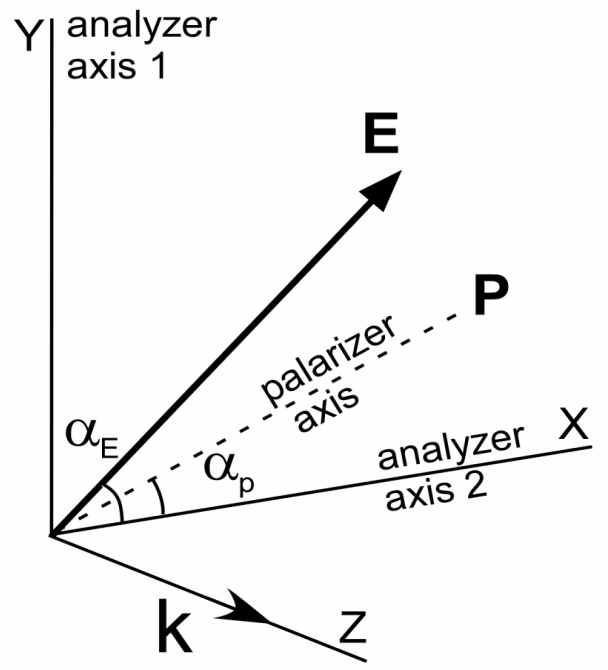

Figure 16: Phase diagram showing the orientation of the polarization set by the Glan prism polarizer to the Electric field in the water and to the polarizations used to form the two images in a Kerr effect electric-field measurement.

Figure 17 demonstrates a set of polarizational images (channel I_Y) of laser-induced breakdown taken on four separate shots: (a) without external voltage; (b) with external voltage prior to laser induced streamer (probing time ~190 ns after voltage start, the voltage ~130 kV, maximum electric field ~433 kV/cm); (c) with external voltage and laser induced streamer head (probing time ~200ns, the voltage ~110kV, maximum electric field ~367 kV/cm); and (d) after breakdown of the water switch gap when voltage drop occurs and current flows through the channel. In all these shots the polarizer angle is $\alpha_P = -20°$. After voltage collapse and start of the current in the gap (Fig. 6-d), the Kerr effect disappears because there is no more significant induced linear anisotropy in the water.

In Sarkisov et al.[26] the intensities in **Fig. 17c** were used to calculate the bulk electric field in the gap and the enhanced field along the streamer head. As a check of the technique, bulk E-fields calculated far away from the streamer along the line from A to A' were calculated, yielding a peak value of ~320 kV/cm. This is in reasonable agreement with the peak electric field of ~300 kV/cm calculated with an electrostatic field solver code[30]. The fields around the streamer head were then calculated along the line from B to B', yielding a peak value of electric field between 1.7 to 2.2 MV/cm, a factor of 6 field enhancement over the peak E-field in the gap without the streamer present. Again, electrostatic field code simulations were performed with a conducting rod in the gap to simulate the streamer. These simulations predicted a factor of 5 enhancement of the bulk E-fields in the gap, in reasonable agreement with the polarization data.

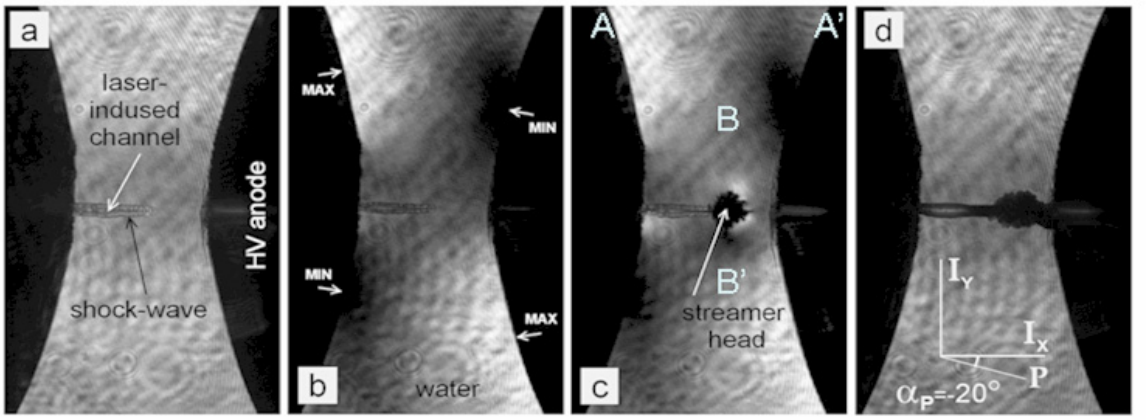

Figure 17: Kerr-effect electric field-measurement images in a 170-kV laser triggered switch showing; a: picture of laser-produced channel with no voltage between the electrodes, b: laser-produced channel in switch with voltage between electrodes showing variation in light intensity caused by bulk E-fields between electrodes, c: Laser-produced channel with breakdown streamer at its head showing variation in light intensity around streamer head caused by local E-field enhancements and d: current-carrying channel after breakdown showing absence of E-fields in switch.

5. Triggering experiments from 0.6 MV to 0.74 MV at the STF facility

Based on the successful triggering results at 170 kV, we designed a series of experiments that could test laser triggering of water switches at voltages from 0.6 MV to 2 MV. Peak current through these switches was on the order of 60 - 100-kA. These experiments allowed us to test laser triggering at "near-full-scale" voltages and currents in a real pulse-power environment. These experiments are taking place at the Sub-Systems Test Facility (STF) in the building 970 High-Bay in Area IV.

5.1 Apparatus

In these experiments, the output of a ~50 KJ Marx generator in oil was shaped by a 670 –nH inductor and a 10-Ohm resistor in series to produce a 600 kV-to-2-MV pulse on a 7.8-Ohm coaxial water pulse-forming line. The risetime of the pulse was set at ~300 ns, to match risetimes on a variety of pulse-power accelerators. The Marx generator had an erected capacitance of 20 nF at a voltage of minus 1.8 MV when the Marx capacitors were charged to voltages of $\pm$ 50 kV. For experiments at ~600 kV, a 20-Ohm shunt resistor to ground was placed across the output of the Marx, just ahead of the 10-Ohm resistor. The Marx generator was typically charged to + 50 kV and the Marx Switches were insulated with 30 - 35 PSIA of dry air.

Figure 18 shows a bottom-view of the 7.8-Ohm coaxial water pulse-forming line (PFL) used in these experiments. This 190-cm-long PFL is similar to the pulse-forming lines used on the RITS accelerator.[8] This PFL had an outer diameter of ~43 cm and an inner diameter of 14 cm. A water switch was located ~106 cm from the input end of the PFL and a matched resistive load was located ~52 cm downstream of the water switch. The water switch electrodes were 7.6-cm diameter hemispheres. One electrode had a central hole to admit the focused laser beam and the other electrode sometimes had a point added to it. An opening above the water switch area allowed experimental access to the water switch. This large opening was closed with a multi-hole splash baffle and a lid when the Marx was operated. Four 10-cm diameter windows were located on the outer wall of the PFL. Two windows on opposite sides of the PFL at the water switch location allowed a diagnostic laser beam to pass through the switch region. Two more windows allowed an unfocused triggering laser beam to be injected through the water, to the inside of the inner PFL, either upstream or downstream of the switch. On the inside of the PFL, the trigger laser entered the "optics can," which was a sealed container at laboratory air, containing windows and focusing optics. **Figure 19** shows a detail of the inside of the inner PFL and the water switch region. The trigger laser entered the "optics can" through a 2-inch-diameter fused silica input window, was focused through either a "long focal length lens" (22-cm fl) or a short focal length lens (8 – 14 cm focal length) exited through a final window and focused through the hole in the cathode to form a breakdown arc between the switch electrodes. For some experiments, "axicon" lenses were used in place of the short focal length spherical lenses to form a line-focus of the laser light in the water between the switches.

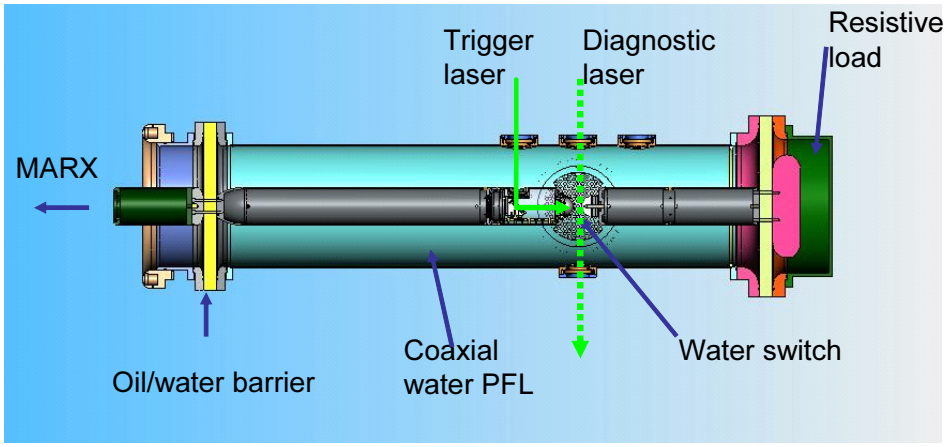

Figure 18: Overview of 2-MV coaxial water pulse-forming line used in 0.6-2 MV laser triggering experiments. Two windows on opposite sides of the water switch region allow a probe laser to apss through the watNote that the probe laser can pass directly through the water switch region through the water switch. The trigger laser passes through one of the other windows to the 'optics can' inside the PFL.

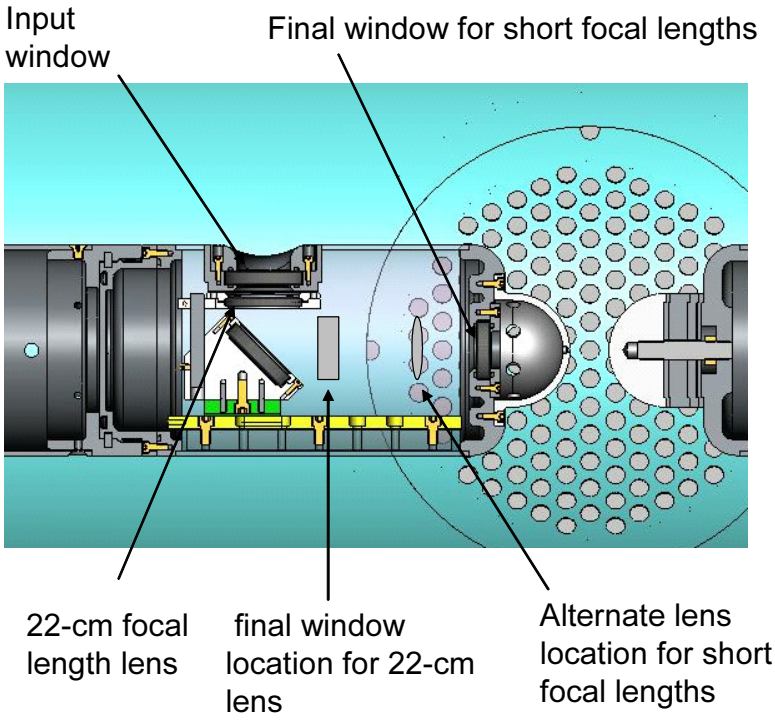

Figure 19: Cut-away view of the 'optics can' inside the PFL. The laser enters through the input window on the top, reflects off the 90^0 turning mirror and is focused by a lens through the hole in the electrode. Alternate lens and final window positions are shown.

We found that it was necessary to use an acrylic lens for the final window when the short focal length lenses were used. A fused silica window was destroyed by the shocks in the water caused by operation of the water switch. It was also necessary to use polycarbonate windows on the 10-cm diameter ports used by the diagnostic laser for the same reason. Both acrylic and fused silica windows were used successfully in the alternate window location when the 22-cm-focal length lens was used.

The laser used to trigger the switch was a frequency-doubled Nd:YAG laser[31] producing ~400 mJ of laser energy at 532 nm in the green in a ~7 ns-long pulse. The trigger laser was typically beam expanded to a 2.0-cm diameter beam by a beam expander on the output of the laser to improve the beam's focusability. The diagnostic laser[32] , which was typically fired 50-100 ns after the trigger laser, was also a frequency-doubled Nd:YAG laser, producing ~80 mJ of energy at 532 nm in a ~7-ns-long pulse. After passing unfocused through the water switch region, the diagnostic laser was relayed ~ 9 meters to the screen box containing the lasers, where it was focused with a 50-cm focal length lens to form an image of the switch electrodes on the face of a CCD camera. ND filters were required to reduce the intensity of the laser by greater than a factor of 10^4 to prevent it from saturating the CCD. This diagnostic laser system produced a ~7-ns-long shadowgram or 'snapshot' of the area between the electrodes at the time the diagnostic laser fired.

The water in the PFL was continuously circulated through a deionizing loop to keep the water resistivity above 1-mega-Ohm-cm. The water was also degassed for some of the experiments.

5.2 Results

5.2.1 Spherical Focusing Lenses

Initial laser-triggering experiments used our 400 mJ green laser focused through lenses with focal lengths ranging from 8 to 22 cm. In these experiments, the gap between the two hemispherical electrodes was 1.9-cm. These experiments were not successful. While the focused laser beam often formed a train of bubbles more than half-way across the switch gap, the switch always broke down at its ~700- kV self-break voltage. The 22-cm-focal length lens formed the longest bubble trains. With the 22-cm lens the switch breakdown would occasionally follow the train of bubbles formed by the laser, but this did not appreciably shorten the breakdown time of the switch. Figure 20 shows two accelerator shots, with a 1.9-cm water gap and a ~640-kV self-breakdown voltage. On shot 311, the bubble train generated by the 22-cm focal-length lens is clearly visible, but the switch appears to be self-breaking along the streamer on the left. In shot 312, the switch broke down along the laser channel. In all of these experiments, the laser beam was brought in upstream of the switch (towards the Marx) and the Marx applied a negative voltage to the PFL.

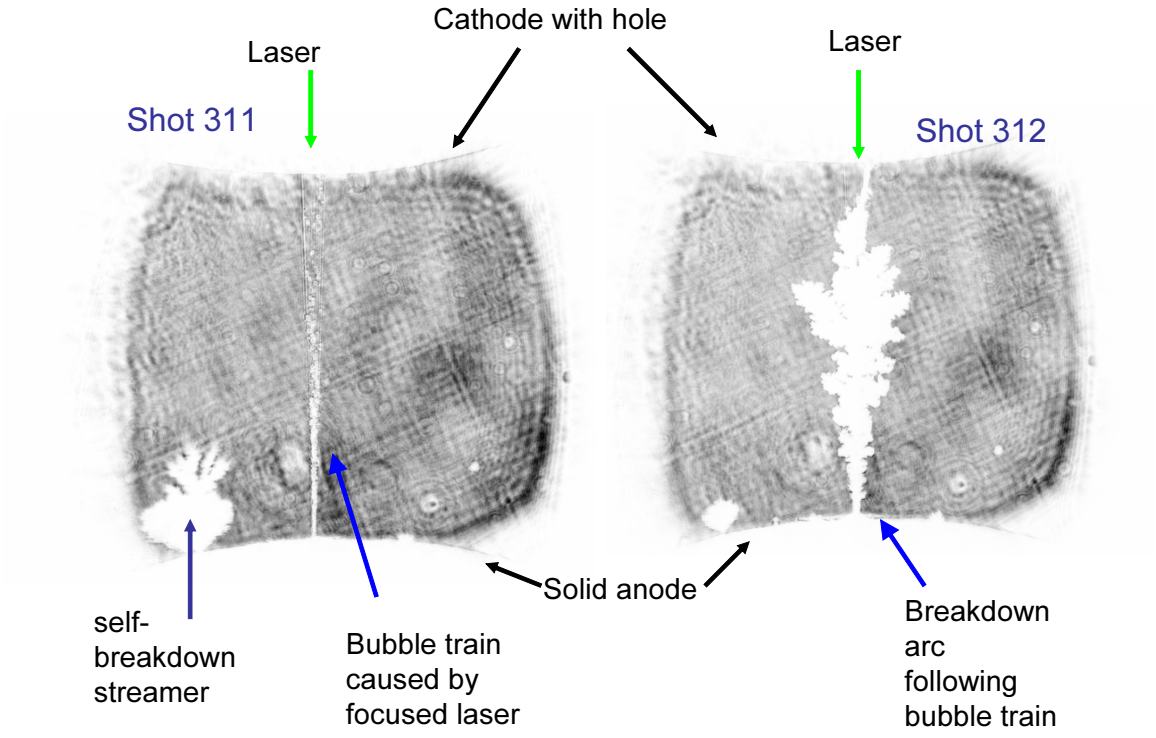

Figure 20: Time-resolved shadowgrams of two different accelerator shots with a 22-cm focal-length focusing lens. The shot on the left self-broke, ignoring bubble train created by the laser, whicle the shot on the right broke down along the bubble train.

5.2.2 Axicon Focusing Lenses

Based on the preceding results, we made three changes to the system: 1) we brought the laser in through the downstream electrode; 2) we put a field-enhanced point for the laser to hit on the cathode and 3) we changed to an axicon[33] lens to focus the laser beam. Unlike spherical lenses, an axicon has a conic cross section. These changes allowed us to consistently laser-trigger the switch. The first two changes allowed the laser to hit a much more highly-enhanced electrode surface. Changing to an axicon lens with a 140^0 cone angle caused the laser to form a line focus rather than a "point" focus. This resulted in a train of bubbles that stretched all the way across the water-switch gap to the enhanced cathode tip. To locate the bubble train between the electrodes, the axicon was moved as close as possible to the gap. Thus, parts of the converging laser beam were still fairly broad when passing through the hole in the anode. To allow the entire laser beam through the electrode, we had to use an anode with a 0.92-cm diameter hole in it. Since laser energy striking near the center of the axicon would have focused inside the final window and damaged it, we put an opaque dot 1.0-cm in diameter on the center of the 2.5-cm diameter axicon. The water-switch gap between the center of the downstream anode and the point on the cathode was 1.9 cm. The point on the cathode extended ~6-mm out from the hemispherical cathode surface. See **figure 21** for details of the axicon setup. The size of the laser beam striking the axicon determined where and how long the bubble train was. Therefore, we adjusted the beam expander on the front of the laser and the size of the opaque dot to optimize the bubble train in the water-switch gap.

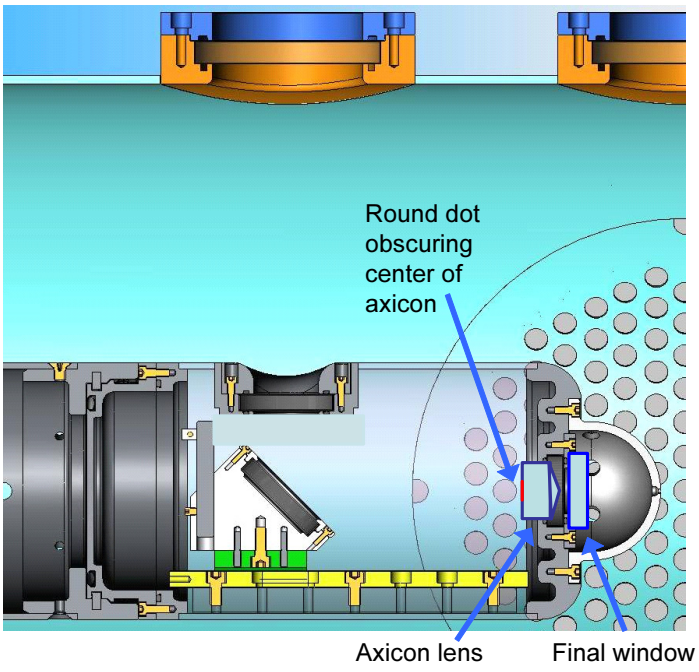

Figure 21: Location of axicon lens and final window for 740-kV laser triggering experiments.

Figure 22 shows a plot of the water switch current and voltage as well as visible light seen by a fiber optic looking in the water switch gap. Scattered light from the trigger laser and diagnostic laser on the fiber light trace give the timing of these two lasers relative to the voltage and current of the switch. We used the information from this type of timing plot to construct the delay versus percent of self-breakdown plots.

Figure 23 shows delay from the trigger laser to switch breakdown versus percent of the switch's 740-kv self break voltage at trigger time for data taken on two different days. A dashed linear fit line is shown through the data. The 1-sigma jitter of the data about this line is $\pm$ 16 ns. This is significantly lower than the $\pm$ 24 ns jitter of the switch in its self-breaking mode. We have two estimates of the laser energy used to produce the triggering results shown in Figure 23. First, the laser energy measured at the outer window of the water PFL was 370 mJ. For our second laser energy estimate, we drained the PFL water and put a calorimeter beyond the focus of the axicon. In this second location, we measured about 220 mJ, indicating that there were significant losses in our optical system inside the PFL.

Figure 24 shows a time sequence of the water gap breakdown assembled from four different shots. In the first frame, 18 ns before switch closure only the laser-produced train of bubbles and a small streamer launched from the sharp point are visible. In the second frame, 10 ns before switch closure, most of the bubble train has broken down, and may have connected to the streamer launched from the point on the cathode. The last few bubbles at the bottom of the picture have not broken down, probably since they are in a relatively low-field region near the 0.92-cm diameter hole in the anode. In the third figure at 0 ns (coincident with the start of the main current pulse in the switch) the bubble train has completely broken down and has connected from the bottom of the bubble train over to the edge of the anode hole. In the final picture at +43 ns, the current through the switch has risen to ~50-kiloAmps.

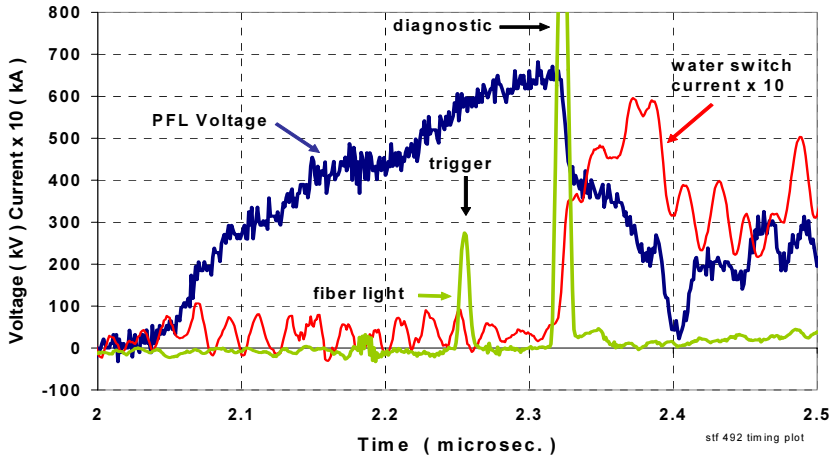

Figure 22: Water switch voltage and current versus time for ?????-cm switch with 740-kV self-break voltage. Scattered light seen by a fiber looking at the gap is used to determine timing of trigger and diagnostic lasers.

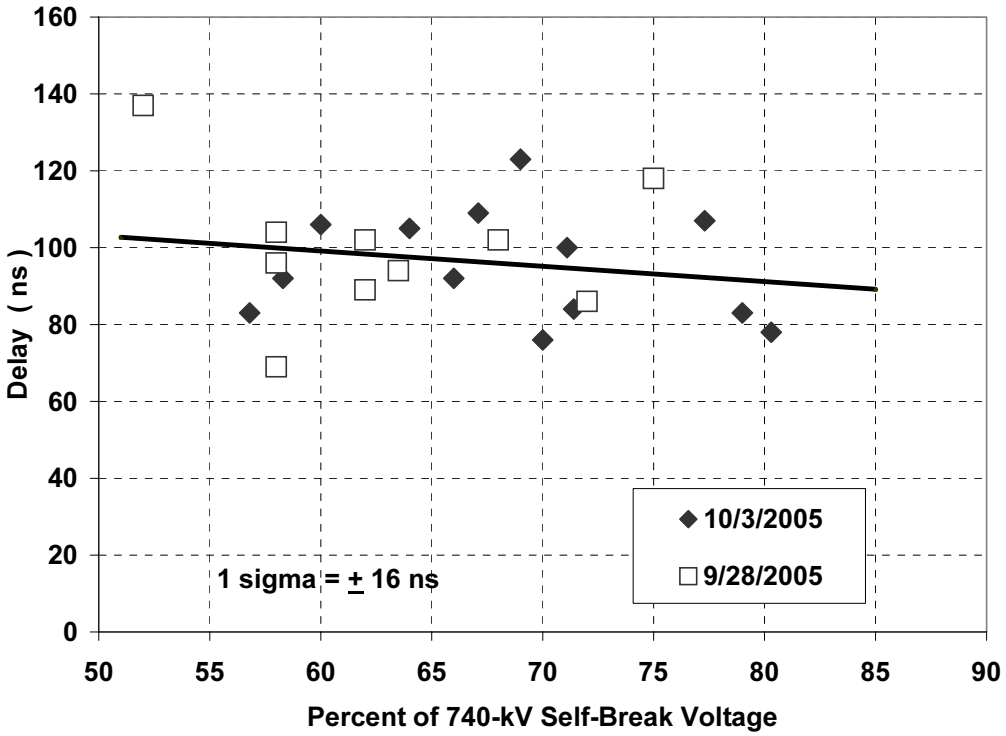

Figure 23: Plot of delay versus percent of self-break voltage at the time the laser triggered the switch for data taken on 2 days with a 740-kV water switch.

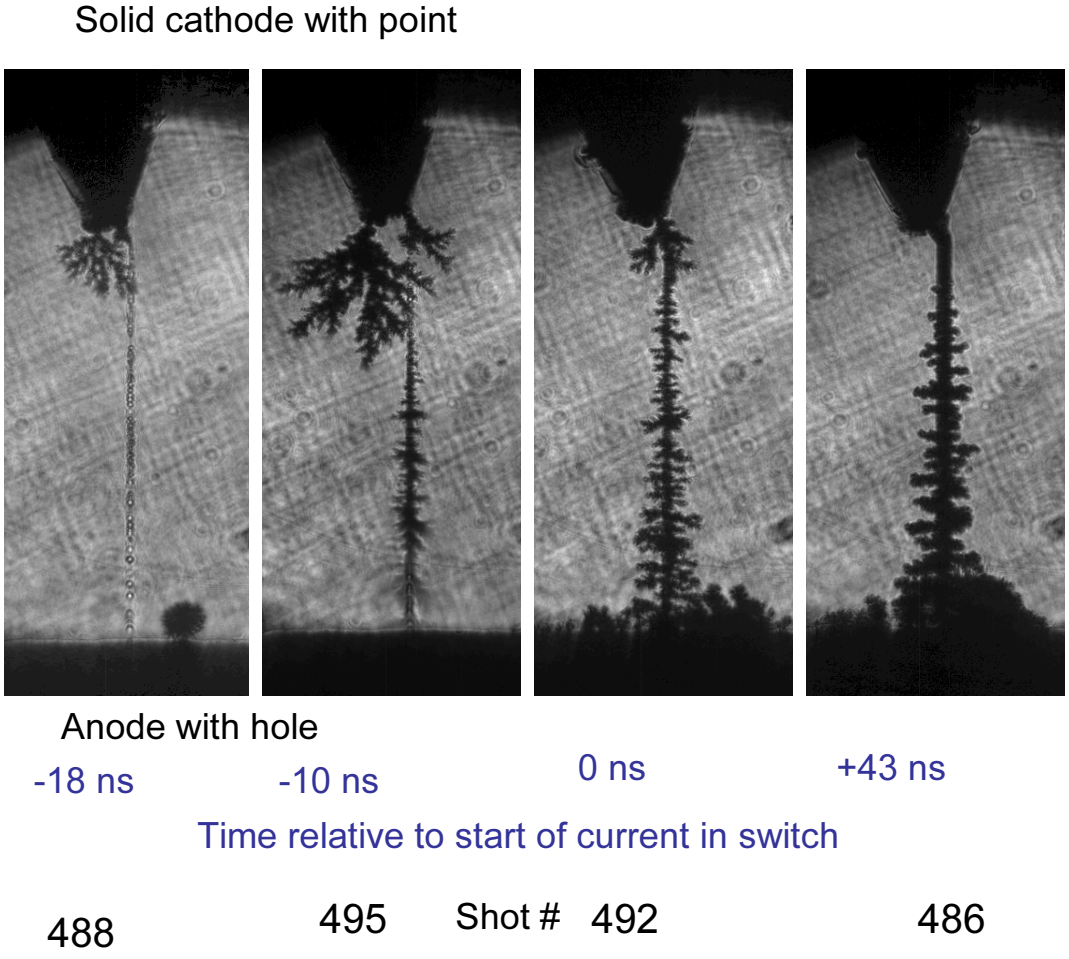

Figure 24: Timing sequence of breakdown of 740-kV laser triggered water switch assembled from four different shots.

5.3 Summary of 740-kV Triggering Results

The shadowgraph pictures (fig. 23) coupled with the curve of delay versus percent of self-breakdown (fig. 24) provide convincing evidence that the laser was triggering the 740-kV water switch when it was focused through the axicon lens. Some of the difference between the + 2 ns jitter obtained in the 170-kV experiments and the +16 ns jitter achieved in the 740-kV experiments can be understood by comparing the laser channels generated in the two experiments. In the absence of switch voltage, the 170-kV switch channels shown in Figs. 7-9 display nearly continuous "dark areas" that probably are a gas column. These are surrounded by overlapping spherical shock waves expanding out from the vapor column. The 740-kV switch channels (before breakdown) shown in figs. 20 and 24 display a chain of isolated bubbles. Given our resolution in the 740-kV pictures, it is not clear whether the "bubbles" we see actually represent the true diameter of the bubbles or whether what we see are actually spherical shock waves expanding out from smaller bubbles inside the shock waves. Thurs, while the 'vapor column' may extend more than 50% the distance from one electrode to the other in the 170-KV experiments, the isolated bubbles of vapor may stretch less than 10% of the distance between electrodes in the 740-kV switch.

In order for laser-triggered water switching to be useful for applications at Sandia National Laboratories, the switch voltage would need to increase to ~2 MV at the same time that the jitter decreased by a factor of two. While this is clearly a challenging goal, the data we presented here represents our first experience with the axicon lens. Further experiments are in progress as a follow-on to this LDRD.

6.0 Acknowledgements:

The authors would like to acknowledge many helpful discussions with Drs. J. Maenchen, D. Bliss, and D. McDaniel at Sandia National Laboratories, Dr. K. Prestwich of Prestwich Consulting and R. Miller of Titan, Pulse Sciences. We are grateful to Mr. D. Nelson of Bechtel, Nevada for his work in installing our data acquisition system. We would like to thank the RITS Accelerator crew for cheerfully putting up with our frequent questions and constant scrounging. Sandia is a multiprogram laboratory operated by Sandia Corporation, a Lockheed Martin Company for the United States Departmens of Energy's National Nuclear Security under contract No. DE-ACO4-94-AL85000.

---

[1] D. L. Johnson, J. P. Vandevender, T. H. Martin, "High Power Density Water Dielectric Switching", IEEE Trans. On Plasma Sci. **PS-**8, pp. 204-209, (1980).

[2] I. Smith, "Pulsed Power in the United States", IEEE Pulsed Power Conf. Record, 15-18, (1991).

[3] F. J. Sazama, "A Streamer Model for High-Voltage Water Switches", IEEE Trans. On Plasma Sci. **PS-8**, pp. 198-203, (1980).

[4] J. P. VanDevender, "The resistive Phase of a High-Voltage Water Spark", J. Appl. Phys, **49**, pp. 2616-2620, (1978).

[5] S. I. Andreev, B. I. Orlov, "Development of a Spark Discharge I", Sov. Phys. Tech. Phys. **1**0, (8), pp. 1097-1101, (1966)

[6] J. R. Woodworth, J. M. Lehr, J. Elizondo-Decanini, P. A. Miller, P. Wakeland, M. Kincy, J. Garde, B. Aragon, W. Fowler, G. Mowrer, J. E. Maenchen G. S. Sarkisov, J. Corley, K. Hodge, S. Drennan, D. Guthrie, M. Navarro, D. L. Johnson, H. C. Ives, M. J. Slattery, D. A. Muirhead, "Optical and Pressure diagnostics of 4-MV Water switches in the Z-20 test facility", IEEE Trans. On Plasma Science, **32**, (5), Oct. 2004, pp. 1778-1789.

[7] T. H. Martin, SB. N. Turman, S. A. Goldstein, J. M. Wilson, D. L. Cook, D. H. McDaniell, E. L. Burgess, G. E. Rochau, E. L. Neau, D. R. Humphreys, "PBFAII, The Pulsed-Power Characterization Phase", IEEE Pulsed Pwr. Conf. Record, pp. 225-228, (1987).

[8] J. E. Maenchen, G. Cooperstein, J. O'Malley and I. Smith, " Advances in Pulsed Power-Driven Radiography Systems" Proc. IEEE,**92**, (7)pp.1024-1042, (2004)

[9] A. H. Guenther, G. L. Zigler, J. R. Bettis, and R. P. Copeland, " Laser triggered switching of a pulsed-charged, oil filled spark gap" Rev. Sci. Instrum., **46**,(7), pp. 914-920, (1975).

[10] B. A. Demidov, M. V. Ivkin, V. A. Petrov, and S. D. Fanchenko, "A high-voltage Water Spark Gap with Laser Firing", Instruments and Experimental Techniques (translation of Pribory i Tekhnika Eksperimenta), **18**,(3), pp. 120-122, (1975).

[11] D. W. Lischer and A. Ramrus, "Laser Initiated Conduction of an Overvolted Water Spark Gap" Proceedings of the 3rd IEEE Pulsed Power Conference, Albuquerque, NM, 1981, pp. 478-481.

[12] E. Chu, P. Korn, D. Lischer, A. R. Miller, A. Ramrus, R. Richardson, M. Wilkinson, J. Shannon, "Advanced Power Source Program Fiscal year 1980", Maxwell Laboratories Inc, Report MLR-1011.

[13] D. A. Vyuga, A. Volkov, P. Tomashevich, G. Baranov, M. J. VanderWiel, G. J. H. Brussaard, "A 2.5 MV subnanosecond pulser with laser triggered spark gap for the generation of high brightness electron bunches," Conf. Record, 14th IEEE International Pulsed Power Conference, Dallas, pp. 867-870, (2003).

[14] H. Buiteveld J. M. H. Hakvoort, M. Donze " The optical properties of pure water" SPIE proceedings on Ocean Optics XII, edited by J. S. Jaffe, 2258, P. 174 (1994).

[15] J. A. Curico and C. C. Petty J. Opt. Soc. America, 41, p. 302 (1951).

[16] G. Herzberg, 'Molecular Spectra and Molecular Structure II, Infrared and Raman Spectra of Polyatomic Molecules' Van Nostrand Reihold Co, New York, p. 240, ISBN 0-442-03386-9.

[17] S. Xiao, J. Kolb, S. Kono, S. Katsuki, R. P. Joshi, M. Laroussi, K. Schoenbach, "High Power Water Switches: Postbreakdown Phenomena and Dielectric Recovery", IEEE Transactions on Dielectrics and Electrical Insulation **11**(4), Aug. 2004, PP. 604-612.

[18] N. F. Bunkin and A. V. Lobeev, Quantum Electronics (translation of Kvantovaya Electronika) **24**,(4) 297-301, (1994)

[19] F. V. Bunkin and V. M. Komissarov, Sov. Phys. Acoustics, **19**, (3) pp. 203-211 (1973).

[20] Q. Feng, J. V. Moloney, A. C. Newell, E. M. Wright, K. Cook, P. K. Kennedy, D. X. Hammer, B. A. Rockwell and C. R. Thompson, "Theory and Simulation on the Threshold of Water Breakdown Induced by Focused Ultrashort Laser Pulses', IEEEJournal of Quantum Electronics **33**(2) Feb. 1997, pp. 127-137.

[21] R. H. Cole, "Underwater Explosions" Princeton Univ. Press, Princeton NJ, 1948, Chapter 8.

[22] V. M. Fedorov " High Power Nanosecond Discharge in Water" Conf. Proceedings, MegaGauss V Conference, Novosibersk, USSR, pp. 319-326 (1989).

[23] M. O. Zahn, E. O. Forster, E. F. Kelley and R. E. Hebner, Jr, "Hydrodynamic Shock Wave Propagation After Electrical Breakdown" Journal of Electrostatics **12**, 1982, pp. 535-546.

[24] Taken from "The Engineering Tool Box" at www.engineeringtoolbox.com/24_159.html

[25] G. S. Sarkisov, J. R. Woodworth, "Measurement of the Current in Water Discharge Using the Magnetooptical Faraday Effect" Submitted to Journal of Applied Physics, 2005.

[26] G. S. Sarkisov, N. D. Zameroski, J. R. Woodworth,"Measurement of Electric Field Enhancement in a Water Streamer using the Electrooptical Kerr Effect", Submitted to Journal of Applied Physics, 2005.

[27] F. C. Jahoda and G. A. Sawyer, in Methods of experimental physics; Vol. 9-B, edited by R. H. Lovberg and H. R. Griem (Academic press, NY, 1971), p. 1-48.

[28] A. Jain, J. Kumar, F. Zhou, et. al., Am. J. Phys, **67**, 714 (1999).

[29] M. Zahn, T. Takada, and S. Voldman, J. Appl. Phys. 54 4749 (1983).

[30] ELECTRO, Software developed by Integrated Engineering Software, Winnipeg, Canada

[31] EKSPLA, LTD, Vilinus, Lithuania.

[32] Tempest laser from New Wave, Inc,

[33] Axicons were procured from Del Mar Ventures, 4119 Twilight Ridge, San Diego, CA 92130, (858)755-6727. http://www.sciner.com/Opticsland/store.htm

DISTRIBUTION:

1 Richard Miller
L-3 Communications Pulse Sciences
4855 Ruffner St., Suite A
San Diego, CA 92111

1 Patrick Corcoran
L-3 Communications Pulse Sciences
2700 Merced St.
San Leandro, CA 94577

1 Ian Smith
L-3 Communications Pulse Sciences
2700 Merced St.
San Leandro, CA 94577

1 Ravindra Joshi
Old Dominion University
Center of Bioelectrics
Kauffman Hall/Room 231
Norfolk, VA 23529

1 Edl Schamiloglu
University of New Mexico
MSC01 1100, Dept EECE
Albuquerque, NM 87131

1 MS 0123 LDRD Office,
Donna Chavez, 1011
1 0335 Juan Elizondo, 2564
1 1106 Frank Wilkins, 1649
1 1178 David Van DeValde, 1639
1 1193 John Maenchen, 1645
1 1193 Jane Lehr, 1645
1 1193 Mark Johnston, 1645
1 1193 Dean Rovang, 1645
8 1193 Joe Woodworth, 1645
1 1193 Nate Zameroski, 1645
1 1193 David L. Johnson, 1645
1 1193 James Blickem, 1645

1 MS 1193 Darryl Droemer, 1649

1 1193 Bob Starbird, 1649

1 1194 Mark Savage, 1644

1 1194 Ken Struve, 1644

1 1194 Gennady Sarkisov, 1644

1 1196 Dan Jobe, 1670

2 0899 Technical Library, 4536

2 9018 Central Technical Files, 8945-1

Sandia National Laboratories